*Bull. Mater. Sci.*, Vol. 40, No. 7, December 2017, pp. 1455–1462
https://doi.org/10.1007/s12034-017-1486-x


# A sensitive optical sensor based on DNA-labelled Si@$SiO_2$ core–shell nanoparticle for the detection of $Hg^{2+}$ ions in environmental water samples

**KRISHNAN SRINIVASAN[1], KATHAVARAYAN SUBRAMANIAN[1], ARULIAH RAJASEKAR[2], KADARKARAI MURUGAN[3], GIOVANNI BENELLI[4,5] and KANNAIYAN DINAKARAN[6,*]**

[1]Department of Chemistry, Anna University, Guindy, Chennai 600 025, India
[2]Department of Biotechnology, Thiruvalluvar University, Vellore 632 115, India
[3]Department of Zoology, Bharathiar University, Coimbatore 641 046, India
[4]Department of Agriculture, Food and Environment, University of Pisa, Via del Borghetto 80, Pisa 56124, Italy
[5]The BioRobotics Institute, Sant'Anna School of Advanced Studies, Viale Rinaldo Piaggio 34, Pontedera 56025, Italy
[6]Department of Chemistry, Thiruvalluvar University, Vellore 632 115, India
*Author for correspondence (kdinakaran.tvu@gmail.com)

MS received 20 October 2016; accepted 2 March 2017; published online 31 October 2017

**Abstract.** Si@$SiO_2$ core–shell nanoparticles were proposed for the development of fluorescent mercury sensor, which also offers a promising alternative to toxic quantum dots (QD)-based heavy metal detection tools. In this study, a sensitive fluorescent assay based on DNA-labelled Si@$SiO_2$ core–shell nanoparticles for the detection of mercury (II) in environmental samples was investigated. Probe DNA was conjugated on the surface of the Si@$SiO_2$ core–shell nanoparticles via 5′-terminal-SH (thiol group) reaction. The detection protocol was based on the DNA hybridization resulted from the formation of mercury-mediated (thymine–$Hg^{2+}$–thymine) base pairs which leave a fluorescent QD on the surface of quartz glass. The synthesized Si@$SiO_2$ core–shell nanoparticle showed a broad emission peak with strong intensity in the UV range around 423 nm. Transmission electronic microscope (TEM) images confirmed the presence of a uniform core–shell structure with Si core nanoparticles with a particle size ranging from 70 to 80 nm and silica shell thickness of about $10 \pm 2$ nm. Overall, our findings highlighted that the developed assay can detect $Hg^{2+}$ ions in aqueous solution as low as 0.92 nM concentration. In addition, the labelled Si@$SiO_2$ core–shell nanoparticles showed prominence sensitivity, acceptable precision, reproducibility and stability, and could be readily applied to environmental sampling systems for $Hg^{2+}$ monitoring.

**Keywords.** Mercury sensor; fluorescent probe; fluorescence sensor; DNA conjugated core–shell nanoparticles; fluorescence resonance energy transfer; quantum dots.

## 1. Introduction

Quantum dots (QDs) are luminescent fluorophores, which attracted huge research attention in biomedical applications and have enormous advantages over traditional organic fluorophores, due to their unique optical properties, such as broad excitation spectra and size tunable emission spectra [1–3]. Semiconductor QDs have been extensively used in biological fluorescence imaging, nanophotonics, sensors and optoelectronic devices [4–6], due to their efficient light emission, quantum yield and photostability. Recently, fluorescence sensors for the detection of mercury based on QDs facilitated fluorescent probe material through $Hg^{2+}$ ions-induced photoluminescence (PL) changes have been reported [7–9]. However, some of the materials are rare in the earth crust. In addition, QDs such as CdS, CdSe, PbSe and $Ag_2S$ are highly toxic to human health and the environment [10]. Consequently, the need of protecting layer over QDs surface is crucial. To reduce the toxic nature of QDs, most of the reported methods are focussed on the application of thiol or acid functionality as a capping material over QDs surface (table 1) [11–16]. Very recently, Xi *et al* [11] focussed on the development of fluorescent mercury sensor based on thiourea-functionalized CdSe/CdS QDs with a detection limit of $0.56\,\mu g\,l^{-1}$. Moreover, Saikia *et al* [12] reported that the PET sensor based on mercaptosuccinic acid (MSA) capped CdTe/ZnS core/shell QD for the detection of mercury and the limit of detection was found to be $1 \times 10^{-12}$ M. Unfortunately, most of these methods demonstrate poor selectivity with interference of some coexisting metal ions such as $Pb^{2+}$, $Ag^{+}$ and $Cu^{2+}$ ions [17].

Unlike other semiconductors' QDs, nanocrystalline silicon has attracted much interest because of its inertness, nontoxic nature, abundance, low-cost and highly biocompatibility [18]. These comprehensive superiorities of silicon create a new possibility for the application of Si nanoparticles in various

**Table 1.** Comparison of the fluorescent nanoparticles and limit of detection (LOD).

| Materials | Method | LOD | Reference |
|---|---|---|---|
| TGA-capped CdSe/CdS | Fluorescence | $0.56\,\mu g\,l^{-1}$ | [11] |
| MSA-capped CdTe/ZnS CS QD | Fluorescence | $1 \times 10^{-12}$ M | [12] |
| GSH-capped CdSe/ZnS | Fluorescence | 10 nM | [13] |
| CA-CdTe QDs | Fluorescence | $0.07\,\mu M$ | [14] |
| MPA-CdTe | Fluorescence | $2.7 \times 10^{-9} mol\,l^{-1}$ | [15] |
| LC-capped CdSe/ZnS | Fluorescence | $1.8 \times 10^{-7}$M | [16] |
| DNA-labelled Si@$SiO_2$ | Fluorescence | 0.92 nM | Present work |

TGA, thioglycolic acid; MSA, mercaptosuccinic acid; GSH, glutathione; CA, cysteamine; MPA, mercaptopropionic acid; LC, L-carnitine.

fields such as chips, memory devices, sensor, energy source, imaging, catalysis, biomedical purposes, electronics and photovoltaics [19–21]. However, silicon is an indirect band-gap semiconductor (1.1 eV), fragile and highly reactive. Thus, bulk silicon does not show efficient light emission, limiting its straightforward applications and leading to an inefficient PL emitter [22,23]. Consequently, to enhance the PL properties of silicon nanocrystals surface treatments, functionalization becomes crucial. Surface modifications include the formation of conductive polymers or organic monolayers on silicon nanocrystals. Among such modifications, the surface oxide coverage is one of the most efficient ways to manipulate the limitations and to obtain band-gap tunable Si QDs [24,25]. Moreover, the hydrophilicity of silicon oxide offers good water dispersibility of the resultant core–shell structure. The physical characteristics of nanoparticles can be tuned by the formation of silica shell and the resultant core–shell structures are more stable due to chemical inertness and optically transparent of the silica shell [26,27]. The desired size and shape of the nanoparticles can also be achieved by controlling the thickness and spatial distribution of shell. In addition, the silica ($SiO_2$) shell on the surface acts as an anchorage platform for hybridization of oligonucleotides. Thus, Si@$SiO_2$ core–shell nanoparticles have been employed for the development of fluorescent mercury sensor, which also offers a promising alternative to toxic QDs (CdS, CdSe and PbSe)-based heavy metal detection.

In this research, to employ core–shell nanoparticle as sensing probe [28], we developed a DNA-functionalized Si@$SiO_2$ core–shell nanoparticles-based optical sensor, employing it for the detection of $Hg^{2+}$ ions in the environmental water analyses. This novel optical mercury biosensor was fabricated using a 'sandwich' detection strategy involving DNA-labelled Si@$SiO_2$ core–shell nanoparticles (i.e., fluorescent probe) and probe DNA. The detection protocol was based on the formation of coordination complex of thymine with $Hg^{2+}$ ions. The results obtained confirm the prominence sensitivity of this approach, which showed a detection limit $<0.82$ nM, if compared to traditional methods currently used for environmental monitoring of mercury.

## 2. Experimental

### 2.1 *Materials and chemicals*

Oligonucleotide (ODN) with a sequence of 5′-SH-$(CH_2)_6$-GTTTCTTCTTTGGTTTGATT-3′ was purchased from Sigma-Aldrich. Quartz glass, 3-glycidoxypropylmethyldiethoxysilane (GPTMS), tetraethyl orthosilicate (TEOS), magnesium powder, hydrochloric acid (HCl), hydrofluoric acid (HF), sodium hydroxide (NaOH), phosphate buffer saline (PBS), polyvinylpyrrolidone (PVP) and metal salts such as $HgSO_4$, $CaCl_2$, $FeCl_3$, $Ni(NO_3)_2$, $Zn(NO_3)_2$, $Pb(NO_3)_2$, $Co(NO_3)_2$, $CuSO_4$, $CdCl_2$, $NiSO_4\,(H_2O)_6$, $CoCl_2$, $AlCl_3$, $CrCl_3$, $AgNO_3$, $AlCl_3$, $K_3Fe[CN]_6$, $HAuCl_4$, $MgCl_2$, $MnCl_4 \cdot 4H_2O$ and $ZnSO_4$ were purchased from SRL, Fischer Scientific and Sigma-Aldrich. The rice husks were collected from local sources in Tamil Nadu, India. All glassware was cleaned successively with aqua regia and deionized water and then dried before use. Milli-Q water was used for all experiments.

### 2.2 *Apparatus*

The fluorescence emission spectra were monitored after the introduction of metal ions into the test assay. The absorption properties of DNA-labelled Si@$SiO_2$ core–shell nanoparticles with various concentrations of $Hg^{2+}$ ions were characterized by using Shimadzu UV-1800 spectrophotometer. JASCO fluorescence spectrometer was used for photoluminescence analysis; the spectra were recorded in the wavelength range of 360–900 nm with an excitation wavelength of 350 nm. The morphology of the Si@$SiO_2$ core–shell nanoparticles was investigated using a Technai10-Philips transmission electron microscope (TEM) at 100 kV. Regular TEM specimens were made by evaporating one drop of the sample solution on carbon-coated copper grids.

### 2.3 *Methods*

2.3a *Synthesis of silicon nanoparticles from rice husk*: The nanosilicon was synthesized from natural sources by

magnesiothermic reaction [29]. In summary, 3 g of raw rice husks were first refluxed with 45 ml of aqueous solution of 10 wt% HCl for 8 h at 60°C to remove the metal ions inside. The leached rice husk was rinsed with deionized water and dried at vacuum at 100°C. Then, the organic components were removed from leached rice husk by calcination in air at 700°C for 3 h to get a white nano-$SiO_2$ powder. Further, about 0.1 g of silica powder was mixed thoroughly with 0.1 g of magnesium powder. The obtained mixture was heated to 650°C for 7 h with a ramping rate of 5°C in a tube furnace at inert atmosphere. After this process, the obtained dark brown powder was etched with 2 M HCl aqueous solution for 6 h followed by soaking in 5% hydrofluoric acid for 10 min to remove unreacted $SiO_2$, MgO and $Mg_2Si$. Finally, the resulting nanosilicon nanoparticles were filtered out rinsed with deionized water and ethanol (4 times) and dried at 80°C over night.

2.3b *Synthesis of Si@SiO$_2$ core–shell nanoparticles and DNA-labelled Si@SiO$_2$ core–shell nanoparticles*: The Si@$SiO_2$ core–shell nanoparticles were synthesized following the Stöber's method [30]. About 100 mg of silicon nanoparticles were dispersed in a mixture of 74 ml ethanol and 10 ml water, using water bath sonication. Subsequently, 0.15 g of PVP and 3 ml of aqueous ammonia (30%) were added into this solution. Finally, 6 ml of TEOS was added dropwise into the solution under vigorous stirring, and the reaction was incubated at room temperature under stirring for 1 h. The resulting Si@$SiO_2$ core–shell nanoparticles were isolated by centrifugation, washed with ethanol and dried. The DNA-immobilized Si@$SiO_2$ core–shell nanoparticles (fluorescent probe) was prepared by mixing 1 mg ml$^{-1}$ solution of GPTMS-functionalized Si@$SiO_2$ nanoparticles with DNA (50 ng ml$^{-1}$) in aqueous phosphate buffer with pH 7.4.

2.3c *Fabrication of quartz glass plates and its optical detection of Hg$^{2+}$ ions by DNA-immobilized Si@SiO$_2$ core–shell nanoparticles*: The quartz glass plates (2 × 0.5 cm) were cleaned thoroughly in an ultra-sonication process using acetone, followed by water. The self-assembled monolayer (SAM) of GPTMS on the pre-cleaned quartz glass plates was prepared by immersing the glass plates in 1% (v/v) GPTMS for 20 h. Subsequently, the plates were dried, and probe DNA was immobilized on the GPTMS-functionalized quartz glass plate and washed with PBS buffer to remove any unbound probe DNA. The fabricated glass plates were then incubated with DNA-immobilized Si@$SiO_2$ core–shell nanoparticles (fluorescent probe) and $Hg^{2+}$ ions. The modified quartz glass plates were analysed with a fluorescence spectrometer. Similarly, the sensitivity of the method was evaluated with various concentrations of $Hg^{2+}$ ions such as 0, 0.2, 0.4, 0.6, 0.8, 1.0, 2.0, 4.0, 6.0, 8.0, 10.0, 20.0, 50.0, 100.0, 200.0, 500.0 and 1000.0 nM, respectively. The specificity of the proposed methods was validated with various metal ions with a fixed concentration 1 μM of metal ions. The metal ions are as follows: $Hg^{2+}$, $Pb^{2+}$, $Cu^{2+}$, $Cd^{2+}$, $Ni^{2+}$, $Co^{2+}$, $Cr^{2+}$, $Ag^{+}$, $Al^{3+}$, $Fe^{3+}$, $Au^{3+}$, $Mg^{2+}$, $Mn^{2+}$, $Zn^{2+}$ and mixture of all these metal ions.

## 3. Results and discussion

### 3.1 *Optical mercury sensor based on labelled Si@SiO$_2$ core–shell nanoparticles*

The labelled Si@$SiO_2$ core–shell nanoparticles (fluorescent probe DNA–Si@$SiO_2$) facilitated fluorescent mercury biosensor was developed based on the sandwich DNA hybridization and is shown in scheme 1. Probe DNA was conjugated on the surface of the Si@$SiO_2$ core–shell nanoparticles through 5′-terminal-SH reaction and the labelled Si@$SiO_2$ core–shell nanoparticles act as a fluorescent probe/molecular recognition (fluorescence resonance energy transfer donor). As shown in scheme 1, probe DNA was immobilized on the GPTMS-functionalized quartz glass plate and subsequently incubated with the $Hg^{2+}$ ions and fluorescent probe. In the absence of $Hg^{2+}$ ions, probe DNA and fluorescent probe were not able to hybridize with each other due to their strong electrostatic repulsion. On the other hand, the presence of $Hg^{2+}$ ions influenced the DNA hybridization resulted from the formation of mercury-mediated (thymine–$Hg^{2+}$–thymine) base pairs and it was used to measure PL spectra to detect the presence of $Hg^{2+}$ ions. Consequently, the acquaintance of fluorescent probe with DNA-immobilized quartz glass plate resulted in the fluorescence enhancement and it was employed to measure PL spectra to detect the presence of $Hg^{2+}$ ions.

### 3.2 *Characterization of Si@SiO$_2$ core–shell nanoparticles and fluorescent probe (DNA-labelled Si@SiO$_2$ core–shell nanoparticles)*

Optical properties of as-prepared Si@$SiO_2$ core–shell nanoparticles were analysed using UV–Vis absorption and PL spectroscopy. The UV–Vis spectrophotometric analysis of Si@$SiO_2$ core–shell nanoparticles and DNA-labelled Si@$SiO_2$ core–shell nanoparticles is shown in figure 1. The absorption maximum peak of Si@$SiO_2$ core–shell nanoparticles was found at 294 nm and the surface plasmon was red-shifted to upon conjugation with DNA probe on core–shell nanoparticles surfaces, confirming the formation of Si@$SiO_2$ core–shell nanoparticles/DNA probe. Similarly, figure 2 provided the PL spectra of Si@$SiO_2$ core–shell nanoparticles and DNA-labelled Si@$SiO_2$ core–shell nanoparticles with a broad and strong intensity in the UV range around 423 nm, which was attributed to quantum size effect along with surface/defect states in the surrounding silicon oxide [29].

The high resolution transmission electron microscope (HRTEM) images of silicon (figure 3a and b) and Si@$SiO_2$ core–shell nanoparticles (figure 3c and d) are provided in figure 3 at different magnifications. From figure 3a and b,

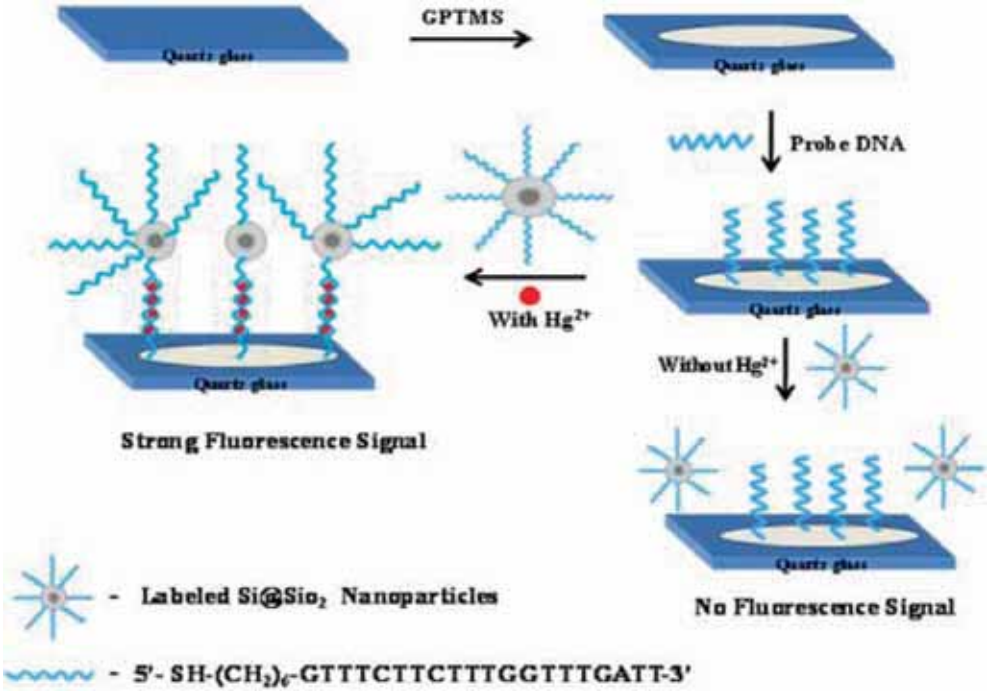


**Scheme 1.** Principle of optical mercury sensor based on labelled Si@$SiO_2$ core–shell nanoparticles.

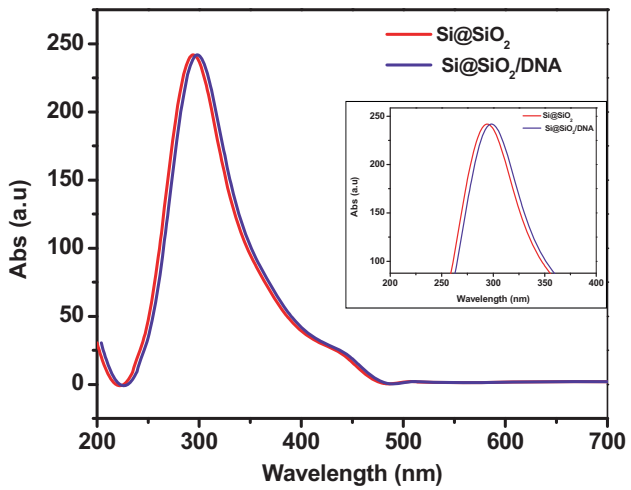


**Figure 1.** UV–Vis spectrophotometric analysis of Si@$SiO_2$ and DNA-labelled Si@$SiO_2$ core–shell nanoparticles (inset: maximized image in the range of 200–400 nm).

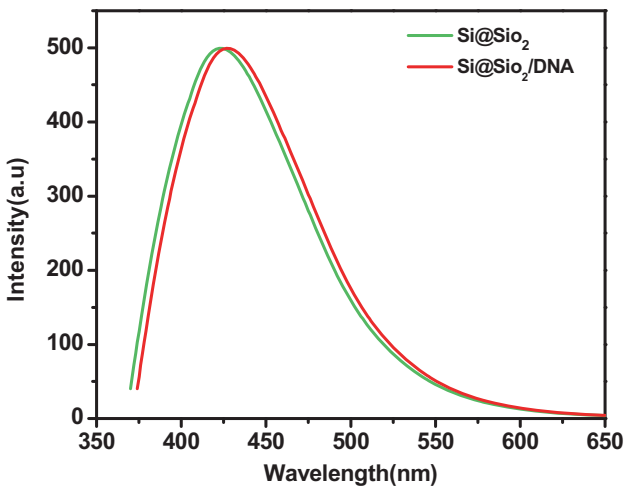


**Figure 2.** PL spectral analysis of Si@$SiO_2$ and DNA-labelled Si@$SiO_2$ core–shell nanoparticles.

the formation of discrete silicon planes was confirmed. Furthermore, under high magnification, the spacing of the lattice fringes of the silicon dots were found consistent with the (111) planes of silicon. It was also observed that the Si core nanoparticles had a size ranging from 70 to 80 nm. However, in core–shell structure, the silica ($SiO_2$) shell cover the core silicon with thickness of about 10 ± 2 nm. The HRTEM images of Si@$SiO_2$ core–shell nanoparticles have demonstrated clearly in figure 3c and d. It was well ascertained in the zoomed out figure that the silicon dots were clearly covered with silica shell. In addition, the X-ray diffractogram of silicon and Si@$SiO_2$ core–shell nanoparticles are presented in figure 4. The peaks at 28.7° (111), 47.7° (220) and 56.4° (311) $2\theta$ are in good agreement with the characteristic peaks of Si with JCPDS card file 65-1060. Further, the formation of silica shell over the nanoparticle surface was also confirmed from the emergence of broad peak at $2\theta = 22°$ in figure 4.

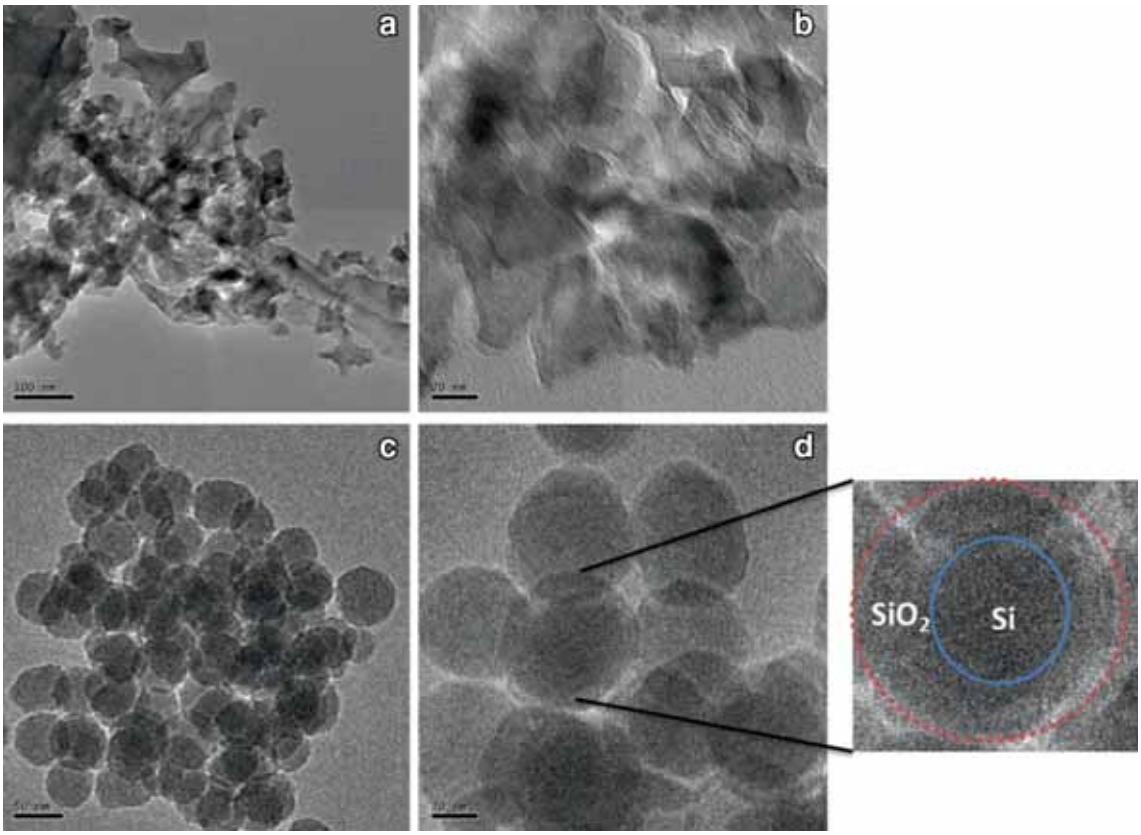


**Figure 3.** HRTEM image of (**a** and **b**) silicon nanoparticles and (**c** and **d**) Si@SiO$_2$ core–shell nanoparticles.

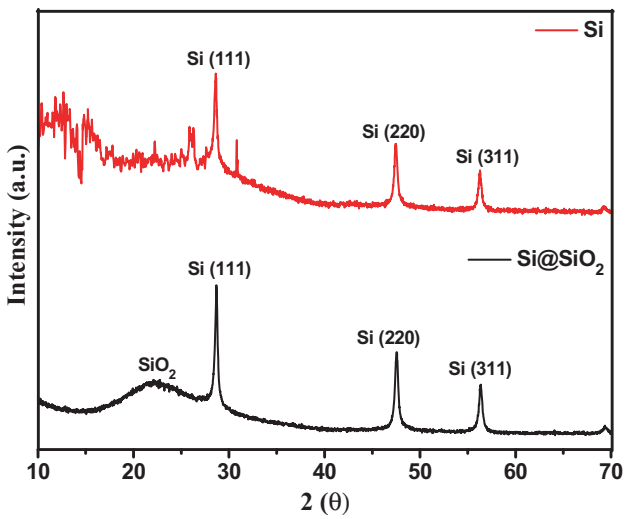


**Figure 4.** XRD pattern of the silicon nanoparticles and Si@SiO$_2$ core–shell nanoparticles.

### 3.3 *Optimization of assay conditions for $Hg^{2+}$ detection*

The sensitivity of the proposed sensor system was based on the concentration of the labelled Si@SiO$_2$ core–shell nanoparticles (fluorescent probe) used in the assay. Various concentrations of fluorescent probe (0–7 μg ml$^{-1}$) were tested to find out the optimum concentration needed to perform the assay. As illustrated in figure 5a, the response intensity of sensor raised when increasing the concentration of fluorescent probe up to 4.0 μg ml$^{-1}$. However, the higher concentration of fluorescent probe from 4 to 7 μg ml$^{-1}$ results in the decrease in the intensity due to the excess binding of the fluorescent probe on the surface which may result in aggregation. Hence, the optimized concentration of labelled Si@SiO$_2$ core–shell nanoparticles was 4.0 μg ml$^{-1}$. Similarly, the effect of pH for the developed fluorescent sensor was evaluated (figure 5b) and the optimized pH was found to be 7.0.

### 3.4 *Optical characterization of modified quartz glass towards the detection of $Hg^{2+}$ ions*

The chronological immobilization of GPTMS, DNA, $Hg^{2+}$ ions and labelled Si@SiO$_2$ core–shell nanoparticles on the quartz glass were characterized by PL and absorbance spectroscopy. Different stages of the PL responses are presented in figure 6. As shown in figure 6, GPTMS, DNA and $Hg^{2+}$ ions-treated glass slide did not show any responses, whereas the treatment of labelled Si@SiO$_2$ core–shell nanoparticles influenced the DNA hybridization. Thus, the broad peak observed at 423 nm resulted from the formation of mercury-mediated (thymine–$Hg^{2+}$–thymine) base pairs. This resulted

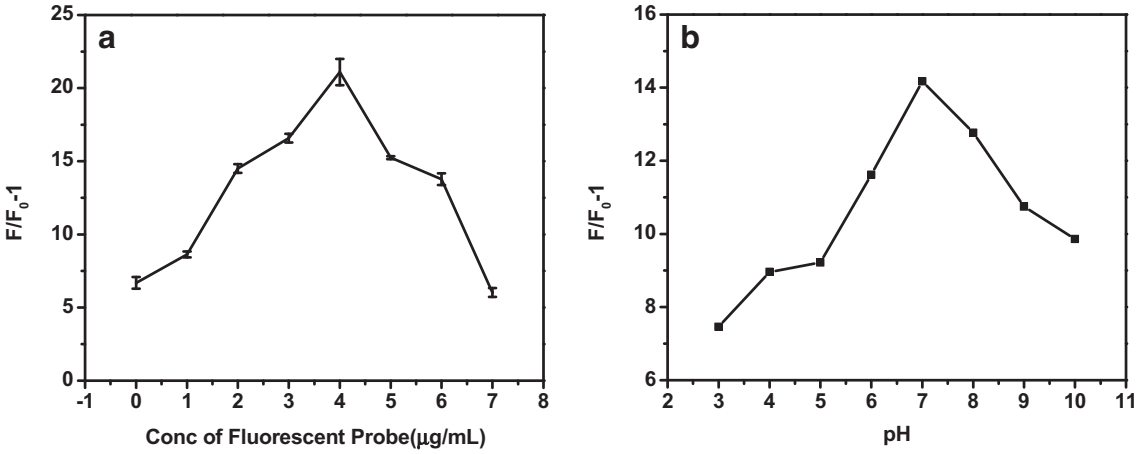


**Figure 5.** (**a**) Effect of concentration of labelled $Si@SiO_2$ core–shell nanoparticles (fluorescent probe). (**b**) Effect of pH on the $F/F_0$-1 value of $Si@SiO_2$ core–shell nanoparticles-based optical sensor. Conditions: 0.1 μM $Hg^{2+}$ ions.

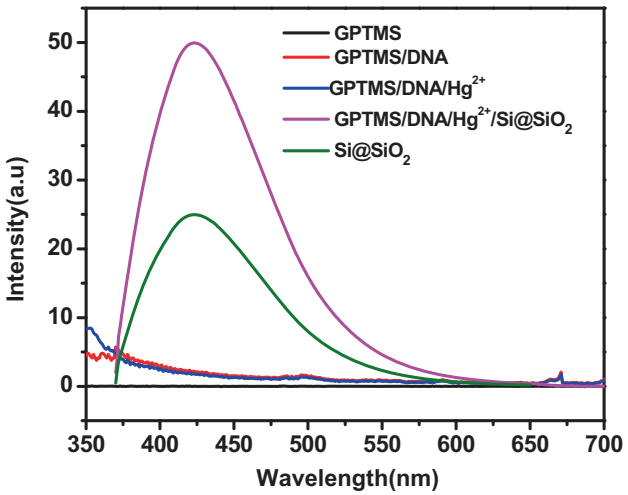


**Figure 6.** PL spectral analysis of modified quartz glass to develop DNA-labelled $Si@SiO_2$ core–shell nanoparticles-based optical mercury sensor.

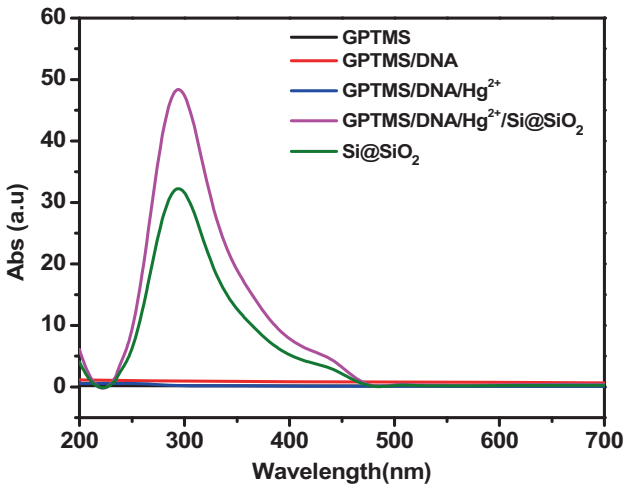


**Figure 7.** UV spectral analysis of modified quartz glass to develop optical mercury sensor based on DNA-labelled $Si@SiO_2$ core–shell nanoparticles.

in intense luminescence peak at 423 nm, which confirms the presence of $Hg^{2+}$ ions on the modified glass plate, but it was not in the absence of the $Hg^{2+}$ ions and a similar observation was also found in the UV–Vis absorbance spectroscopy (figure 7). The emergence of an intense PL is attributed to a specific detection of $Hg^{2+}$ ions on the DNA-functionalized glass surface and followed by the treatment with the labelled $Si@SiO_2$ core–shell nanoparticles. Therefore, the obtained UV–Vis and PL spectrum confirmed that the different species were sequentially immobilized on the GPTMS-functionalized quartz glass. Furthermore, there was no response in fluorescence emissions or absorbance for the bare and untreated $Hg^{2+}$ ions quartz glass, which revealed that the appearance of a peak was not due to the nonspecific and physical adherence of the fluorescent probe on the modified quartz glass surface.

### 3.5 *Sensitivity and detection limit of the DNA-labelled $Si@SiO_2$ core–shell nanoparticles-based optical sensor towards the detection of $Hg^{2+}$ ions*

The quantitative detection of $Hg^{2+}$ ions of the developed optical sensor was examined with different concentrations of $Hg^{2+}$ ions under the optimized condition and the corresponding PL spectra were recorded. The optical responses for various concentrations of $Hg^{2+}$ ions (0.2, 0.4, 0.6, 0.8, 1.0, 2, 4, 6, 8, 10, 20, 50, 100, 500 and 1000 nM) are shown in figure 8. It was observed that the fluorescence intensity increased linearly with increasing concentration of $Hg^{2+}$. Thus, the emission peak was enhanced proportionate to the concentration of $Hg^{2+}$ ions and the detection limit of $Hg^{2+}$ ions was 0.92 nM. Standard graph of PL intensity *vs.* the concentration of $Hg^{2+}$ ions using the proposed method is

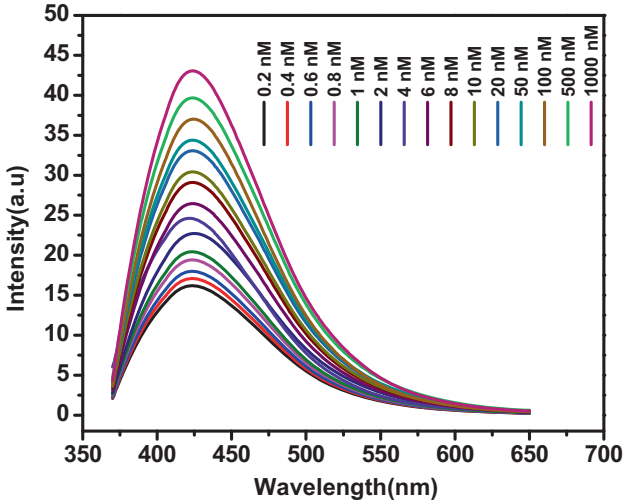


**Figure 8.** PL analysis of DNA-labelled Si@SiO$_2$ core–shell-based optical sensors with various concentrations of $Hg^{2+}$ ions from (top to bottom) 0 to 1000 nM.

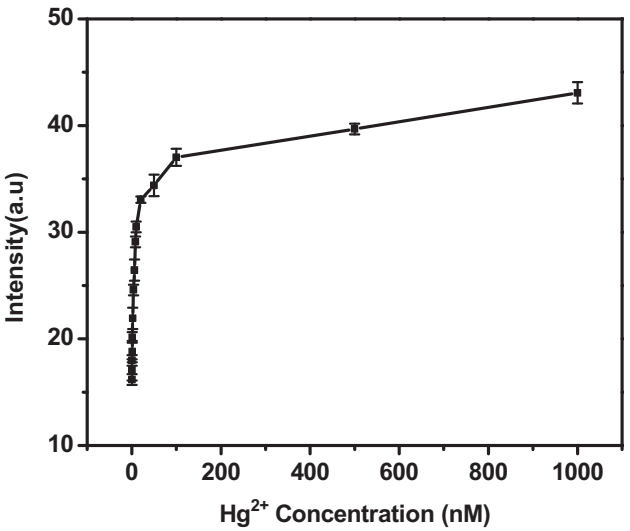


**Figure 9.** Standard graph of PL intensity *vs*. the concentration of $Hg^{2+}$ ions DNA-labelled Si@SiO$_2$ core–shell-based optical sensor.

presented in figures 9 and 10, which revealed a good linear correlation between F/F0-1 and the concentration of $Hg^{2+}$ ions in the range of 0–10 and 0–1 nM and their respective coefficients of determination were 0.98815 and 0.99551, respectively. The developed method demonstrates nonlinear nature in the range of 0–1000 nM; such behaviour may be caused by the free Si@SiO-$_2$ core–shell nanoparticles (figure 10). However, the most linearity was found with minimum concentration alone. The reproducibility of the developed optical sensor was assessed by a series of five assays under optimized conditions to detect 50 nM of $Hg^{2+}$ ions and the respective coefficient variations of the assay were 3.2%, which highlighted that the assay is reproducible in optimized conditions.

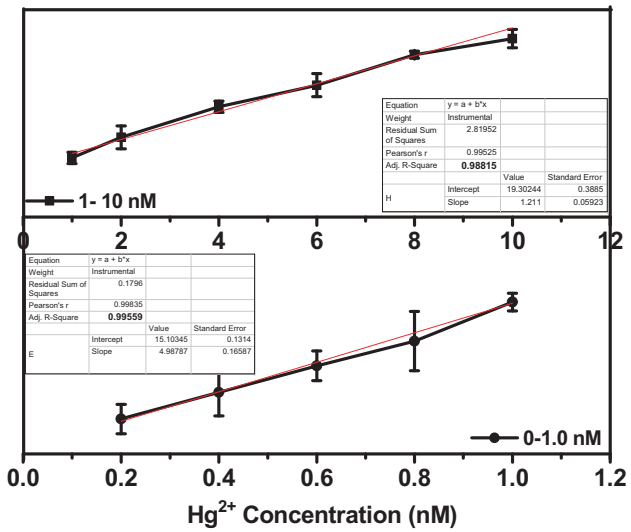


**Figure 10.** Linear region of standard graph of DNA-labelled Si@SiO$_2$ core–shell-based optical sensors. The concentrations of $Hg^{2+}$ ions were 0, 0.2, 0.4, 0.6, 0.8, 1.0, 2.0, 4.0, 6.0, 8.0 and 10 nM.

### 3.6 *Validation of specificity of the DNA-labelled Si@SiO$_2$ core–shell nanoparticles-based optical sensor towards the detection of $Hg^{2+}$ ions*

The selectivity of the present method was evaluated in comparison with other environmentally relevant heavy metal ions including $Hg^{2+}$, $Pb^{2+}$, $Cu^{2+}$, $Cd^{2+}$, $Ni^{2+}$, $Co^{2+}$, $Cr^{2+}$, $Ag^{+}$, $Al^{3+}$, $Fe^{3+}$, $Au^{3+}$, $Mg^{2+}$, $Mn^{2+}$, $Zn^{2+}$ and mixed ions at a concentration of 10 μM. As evident from figure 11, only the presence of $Hg^{2+}$ ions induced a dramatic increase in fluorescence intensity, whereas the presence of other cations does not show obvious fluorescence changes. Consequently, the fluorescence intensity was apparently higher over that of other samples without $Hg^{2+}$ ions, which indicates that the proposed sensor system had a high selectivity towards $Hg^{2+}$ ions against other metal ions. The good performance of selectivity results from the specific coordination between T bases and $Hg^{2+}$ ions.

### 3.7 *Evaluation of the applicability and reliability of the developed optical mercury sensor in environmental water samples*

The applicability and reliability of the developed fluorescent mercury sensor were evaluated with the recovery experiments of different $Hg^{2+}$ ion concentrations in real water samples that were collected from local water resources and tap water. To remove impurities, the water samples were centrifuged and diluted 10 times with 100 mM PBS. Further, various concentrations of $Hg^{2+}$ ions (2.0, 5.0, 10.0 and 50.0 nM) were spiked with the water samples and analysed. From the obtained results (table 2), it is noted that the recoveries for the added $Hg^{2+}$ ions with 3.0, 6.0, 10.0 and 50.0 nM are 99.6,

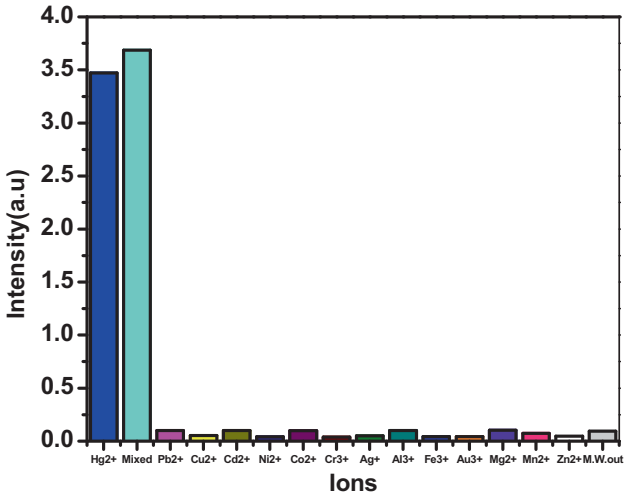


**Figure 11.** Selectivity of DNA-labelled $Si@SiO_2$ core–shell nanoparticles-based optical sensor system for the detection of $Hg^{2+}$ ions in the presence of other metal ions. The concentrations of $Hg^{2+}$ ions and other metal ions are 0.1 and 1.0 μM, respectively.

**Table 2.** Recovery assays of $Hg^{2+}$ ions in environmental water samples using the developed optical mercury sensor.

| Sample | Added $Hg^{2+}$ (nM) | Found (nM) | Recovery (%) |
|---|---|---|---|
| Water 1 | 03 | $2.99 \pm 0.15$ | 99.6 |
| Water 2 | 06 | $6.15 \pm 0.28$ | 102.5 |
| Water 3 | 10 | $9.75 \pm 0.33$ | 97.5 |
| Water 4 | 50 | $49.95 \pm 0.59$ | 99.9 |

102.5, 97.5 and 99.9%, respectively. These results revealed that the recovery of the developed fluorescent mercury sensor was satisfactory and reliable in determining trace amount of $Hg^{2+}$ ions in real environmental samples.

## 4. Conclusions

Generally, DNA-labelled $Si@SiO_2$ core–shell nanoparticle-facilitated fluorescent sensor was developed towards the detection of heavy metal $Hg^{2+}$ ions in the environmental water samples. The sensitivity of the developed assay was higher due to the more binding sites available for $Hg^{2+}$ ions on the fluorescent probe. It was affirmed and demonstrated that the DNA-labelled $Si@SiO_2$ core–shell nanoparticle-based fluorescent mercury sensor has higher sensitivity and specificity with detection limit as low as 0.92 nM. Consequently, the projected DNA-labelled $Si@SiO_2$ core–shell nanoparticle-facilitated fluorescent sensor assay stands for high sensitive, specificity, easier processing, cost competitive and higher recovery percentages for the detection of a trace amount of $Hg^{2+}$ ions in real environmental samples.

## Acknowledgements

Dinakaran acknowledges the financial support from Department of Science and Technology, India, through Fast Track Young Scientist Scheme: Grant no. SR/FT/CS-103/2009.

## References

[1] Prasad P N 2004 (New York: Wiley-Interscience)
[2] Alivisatos A P 1996 *Science* **271** 933
[3] Eckhoff D A, Sutin J D B, Clegg R M and Gratton E 2005 *J. Phys. Chem. B* **109** 19786
[4] Li Z F and Ruckenstein E 2004 *Nano Lett*. **4** 1463
[5] Warner J H, Hoshino A, Yamamoto K and Tilley R D 2005 *Angew. Chem. Int. Ed*. **44** 4550
[6] Tilley R D and Yamamoto K 2006 *Adv. Mater*. **18** 2053
[7] Liu S, Shi Z, Xu W, Yang H, Xi N, Liu X *et al* 2014 *Dyes Pigm.* **103** 145
[8] Yan F, Zou Y and Wang M 2014 *Sens. Actuators B* **192** 488
[9] Xie W Y, Huang W T, Luo H Q and Li N B 2012 *Analyst* **137** 4651
[10] Kang Z, Liu Y, Tsang C H A, Ma D, Fan X, Wong N B *et al* 2009 *Adv. Mater*. **21** 661
[11] Xi L L, Ma H B and Tao G H 2016 *Chin. Chem. Lett*. In Press. https://doi.org/10.1016/j.cclet.2016.03.002
[12] Saikia D, Dutta P, Sarma N S and Adhikari N C 2016 *Sens. Actuators B* **230** 149
[13] Freeman R, Finder T and Willner I 2009 *Angew. Chem. Int. Ed*. **48** 7818
[14] Pei J, Zhu H, Wang X, Zhang H and Yang X 2012 *Anal. Chim. Acta* **757** 63
[15] Duan J, Song L and Zhan J 2009 *Nano Res*. **2** 61
[16] Li H, Zhang Y, Wang X and Gao Z 2008 *Microchim. Acta* **160** 119
[17] Ding X, Qu L, Yang R, Zhou Y and Li J 2015 *Luminescence* **30** 465
[18] Dong H, Hou T, Sun X, Li Y and Lee S T 2013 *Appl. Phys. Lett*. **103** 123115
[19] Koshida N and Matsumoto N 2003 *Mater. Sci. Eng. R* **40** 169
[20] Hirschman K D, Tsybeskov L, Duttagupta S P and Fauchet P M 1996 *Nature* **384** 338
[21] Meier C, Gondorf A, Lüttjohann S, Lorke A and Wiggers H 2007 *J. Appl. Phys.* **101** 103112
[22] Joo J, Cruz J F, Vijayakumar S, Grondek J and Sailor M J 2014 *Adv. Funct. Mater*. **24** 5688
[23] Kanemitsu Y, Iiboshi M and Kushida T 2000 *J. Lumin*. **87–89** 463
[24] Lin S W and Chen D H 2009 *Small* **5** 72
[25] Prucnal S, Cheng X Q, Sun J M, Kögler R and Skorupa W 2005 *Vacuum* **78** 693
[26] Li T, Zhou Y, Sun J and Wu K 2012 *Am. J. Anal. Chem*. **3** 12
[27] Yang Y H and Gao M Y 2005 *Adv. Mater*. **17** 2354
[28] Srinivasan K, Thiruppathiraja C, Subramanian K and Dinakaran K 2014 *RSC Adv*. **4** 62399
[29] Xing A, Tian S, Tang H, Losic D and Bao Z 2013 *RSC Adv*. **3** 10145
[30] Yang L Y, Li H Z, Liu J, Sun Z Q, Tang S S and Lei M 2015 *Sci. Rep*. **5** 10908